Attenuation of Radar Signal by a Boreal Forest Canopy in Winter

Juha Lemmetyinen, *Member, IEEE*, Jorge Jorge Ruiz, Juval Cohen, Jouko Haapamaa, Anna Kontu, Jouni Pulliainen, *Senior Member, IEEE*, and Jaan Praks, *Member, IEEE*

***Abstract*— An investigation of boreal forest attenuation of a radar signal in winter is presented, applying a multifrequency (1–10 GHz) ground-based synthetic aperture radar (GB-SAR). As stable targets, corner reflectors (CRs) with known radar cross section (RCS) were used under the forest canopy. This enabled to relate changes in observed wideband backscattering from the reflectors to attenuation of the radar signal in forest vegetation, eliminating the influence of the background, such as snow and soil. We found that ambient temperature affected the observed attenuation of the radar signal in the entire 1–10-GHz frequency range. For temperatures $T < 0$ °C, attenuation was found to decrease by up to 4.3 dB at the lowest observed temperatures of −36 °C, with peak attenuation occurring at $T \approx 0$ °C. The overall apparent two-way attenuation increased by up to 18 dB from L- to X-band. The presence of snow on the canopy was found to increase attenuation by 1–4 dB, the effect increasing with frequency while having only negligible effects on vegetation backscatter.**

***Index Terms*— Boreal forest, ground-based synthetic aperture radar (GB-SAR).**

I. Introduction

MICROWAVE remote sensing using radar at suitable frequencies is useful in retrieving structural properties of forest vegetation such as biomass [1], [2]. Usual radar frequencies penetrate the forest canopy while interacting with its different structural components, such as needles, leaves, branches, and tree trunks; the applied wavelength determines which components most affect electromagnetic waves propagating through the canopy (e.g., [3]). The sensitivity of the signal to structural components depends also on the applied polarization combination: e.g., at L-band, horizontal transmit horizontal receive (HH)-pol(arized) backscattering has been found to be dominated by trunk-ground double-bounce interactions, horizontal transmit vertical receive (HV) pol by volume scattering, and vertical transmit vertical receive (VV) pol by a mixture of these components [2].

Manuscript received 21 March 2022; revised 5 June 2022; accepted 19 June 2022. Date of publication 29 June 2022; date of current version 14 July 2022. This work was supported in part by the Academy of Finland under Grant 325397, in part by the Scientific Advisory Board for Defence, Finland, and in part by the European Space Agency under Contract 4000131497/20/NL/CT. *(Corresponding author: Juha Lemmetyinen.)*

Juha Lemmetyinen, Jorge Jorge Ruiz, Juval Cohen, Anna Kontu, and Jouni Pulliainen are with the Finnish Meteorological Institute, 00560 Helsinki, Finland (e-mail: juha.lemmetyinen@fmi.fi).

Jouko Haapamaa is with the Finnish Defence Research Agency, 34110 Lakiala, Finland.

Jaan Praks is with the Department of Electronics and Nanoengineering, Aalto University, 00076 Espoo, Finland.

Digital Object Identifier 10.1109/LGRS.2022.3187295

In addition to vegetation structure, the dielectric properties of the vegetation tissue in relation to the surrounding medium determine the strength of the scattering and absorption mechanisms, yielding direct relations between radar backscattering intensity and vegetation water content (e.g., [4]). In winter, recent studies using passive microwave sensors have revealed the sensitivity of microwave transmissivity of vegetation to changes in ambient temperature with a distinct increase of transmissivity [or equivalent decrease in vegetation optical depth (VOD)] in freezing conditions [5], [6]. This dependency was hypothesized to be related to biological protection mechanisms in Northern tree species: the vegetation tissue does not freeze uniformly in subzero temperatures, but freezing takes place gradually, being controlled by extracellular freezing processes affecting ice nucleation temperature up to −40 °C [7], [8].

We present the results of an experiment using a ground-based synthetic aperture radar (GB-SAR) operated from L- to X-band (1–10 GHz) [9], examining the effect of environmental parameters on forest canopy attenuation. The canopy attenuation was estimated by observing σ_0 (backscattering coefficient) of stationary corner reflectors (CRs) placed under the forest canopy. The results show a distinct relation between tree temperature and apparent attenuation of the canopy in freezing conditions, confirming earlier results obtained using passive microwave radiometry for a new frequency range and sensor type. Backscatter observed directly from bare ground and the forest canopy also shows distinct differences in response to temperature at different bands.

Section II presents the experimental setup and Section III presents the main results of the study. Discussion and conclusion are given in Section IV.

II. Experimental Setup

A. Measurement Area

The measurement setup was implemented at the Finnish Meteorological Institute Arctic Space Center, Sodankylä, Finland, for the winter of 2020–2021. The setup is shown in Fig. 1. The SodSAR (Sodankylä Synthetic Aperture Radar) instrument (see Section II-B) was installed on a platform at a height of 19 m overlooking a sparse coniferous forest. The imaged measurement area was an approximately 30 × 50 m^2 section of a forests stand consisting almost uniquely of Scots pine (Pinus sylvestris). The forest was characterized

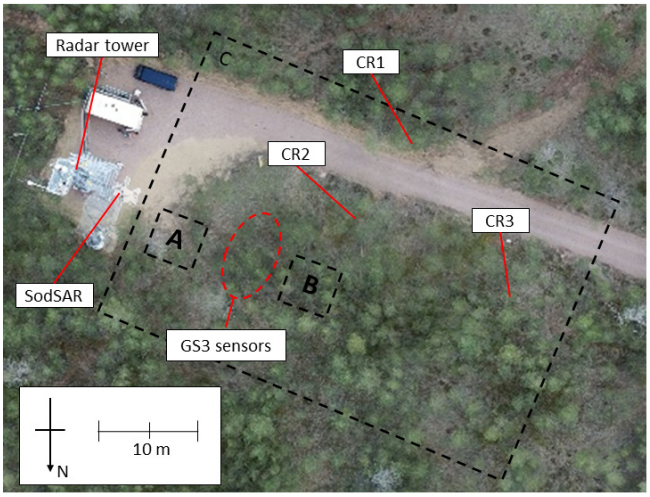

Fig. 1. Aerial orthophotograph of test area. Location of radar tower, SodSAR, CRs 1-3, and location of GS3 *in situ* sensors measuring tree properties indicated. An area representative of bare ground (A), forest (B), and the total area covered by the collected SAR images (C) indicated by dashed lines. Locations and distances are approximate.

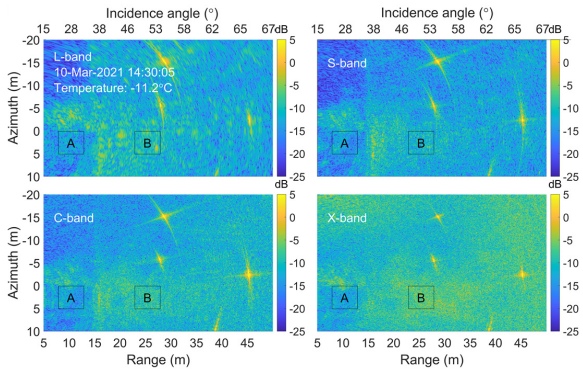

Fig. 2. Examples of focused SodSAR VV-pol σ_0 from L- to X-band on March 10, 2021. Areas A and B identified. CRs visible as radiometrically bright targets.

in the summer of 2018 by measuring the diameter at breast height (DBH) and total height of trees ($N = 1035$). The mean tree height was 10.5 ± (standard deviation) 2.2 m, with an average DBH of 9.3 ± 3.6 cm, yielding a mean biomass of 25.4 ± 30 kg/m^2 [10]. Sections representing bare ground and a forest canopy are identified in Fig. 1 (Areas A and B, respectively), as well as the approximate location of reference targets (CRs, see Section II-C).

B. SodSAR

SodSAR is a 1–10 GHz continuous-wave, fully polarimetric frequency scanning GB-SAR system [10]. The system includes a displacement rail enabling to move the antenna on a 5-m horizontal aperture. Using the displacement capability, SodSAR can be used to generate synthetic aperture radar (SAR) images while applying the time-domain backprojection method for image focusing in range. In this study, VV-pol images were generated at four discrete 1-GHz bands representing L- (1–2 GHz), S- (2.5–3.5 GHz), C- (5–6 GHz), and X-band (9–10 GHz). Only VV-pol was measured to minimize time for SAR operation. Radiometric stability of SodSAR was monitored by observing an unobstructed trihedral CR.

For this study, SodSAR was operated from October 16, 2020 to April 31, 2021. A total of 601 images at VV-polarization were collected, nominally every 6 h. However, several maintenance breaks interrupted data collection. The entire 5-m aperture was used, measuring along the rail in 2-cm increments (250 samples). The 1-GHz observing band yielded a range resolution of ca. 19 cm at a distance of 25 m (Area B). Azimuth resolution at the same distance was from 9 cm at X-band to 51 cm at L-band. The images were projected on a 10×10 cm^2 equal-area grid at ground level. Fig. 2 shows the examples of focused SAR images on March 10, 2021 before radiometric calibration. Areas A and B are identified, the CRs appearing as objects with high σ_0. The incidence angle ranged from 28° for Area A to 67° for the furthest CR. Averaged over an area of 5×5 m^2, the number of looks over Area A(B) ranged from 370(260) at L-band to over 2000 (1480) at X-band. Absolute calibration of the image using the present setup proved challenging due to measurement geometry and having only a single unobstructed reflector. Consequently, all analyses are performed considering relative changes in the backscattering response.

C. Reference Targets

Three trihedral CRs with an aperture width of 90 cm were set up in the test area. One reflector (CR1) was installed along the access road (see Fig. 1), providing an unobstructed line of sight to the radar. CR1 was used for ascertaining instrument stability and as a reference to other CRs for calculating vegetation attenuation. Another two reflectors (CR2 and CR3) were installed under the canopy, positioning the reflectors so that several trees of varying size were in the line of sight between the radar and each reflector.

The purpose of the setup was to monitor possible changes in the observed σ_0 from CR2 and CR3, comparing these to σ_0 from CR1, and attributing changes in the difference to attenuation and backscattering properties of the canopy (see Section II-B). The nominally high radar cross section (RCS) of the CRs provides a relatively stable and strong backscattering signal, typically exceeding the magnitude of σ_0 of the surrounding landscape by over 10 dB, even in the case of reflectors located under the canopy. σ_0 of CRs was calculated by integrating over image pixels providing at least half of the observed peak backscatter over a 9-m^2 area at the assumed location of the CR. Contribution to σ_0 from the background was subtracted using σ_0 of an equivalent area of Area A. The location of the CRs was used to calculate relative differences in gain of the transmitting and receiving antennas of SodSAR, providing a bias correction for the calculated σ_0 of each CR.

D. Ancillary Data

Several sensors measuring the temperature of the tree surface and dielectric properties of the vegetation tissue were installed in the target area. The sensors (METER Group GS3), originally designed for measurement of soil volumetric water

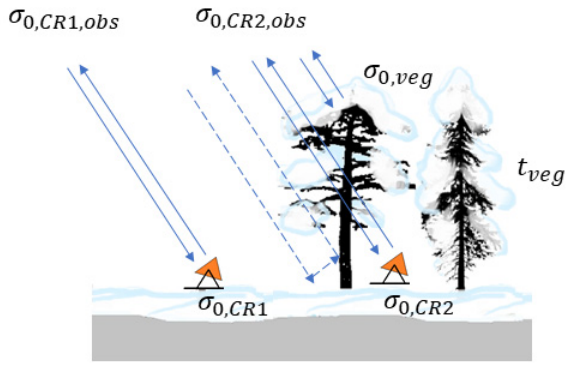

Fig. 3. Schematic of setup for measuring canopy transmissivity t_{veg} using two CRs with identical $\sigma_{0,\text{CR1}} = \sigma_{0,\text{CR2}}$. Scots pine artwork Ian Burt, 2007.

content, were installed on representative tree specimens of varying age and diameter at a height of 2 m from ground level. The dielectric measurement frequency of the sensors is 70 MHz. A total of nine sensors were mounted on six trees in a 15 m radius, with four sensors on a single tree at different locations. In addition, air temperature, ground temperature at 10 cm depth, and snow depth (SD) on ground were measured by separate sensors. A camera was installed to monitor the test area from the radar tower. Images taken at noon (UTC) were collected and used to assess the daily presence of snow on the forest canopy. The canopy was visually classified to be either snow free or laden with light or heavy snow.

E. Calculation of Canopy Attenuation

The two-way attenuation of the radar signal was calculated by adapting a zeroth-order approximation [11]. The total σ_0 observed from a CR under the forest canopy $\sigma_{0,\text{CR,obs}}$ can be approximated as

$$\sigma_{0,\text{CR,obs}} = t_{\text{veg}}^2 \cdot \sigma_{0,\text{CR}} + \sigma_{0,\text{veg}}\left(1 - t_{\text{veg}}^2\right) \tag{1}$$

where t_{veg} is the one-way transmissivity of vegetation, $\sigma_{0,\text{CR}}$ is the backscattering coefficient of an unobstructed CR at the ground level (ignoring the contribution of ground backscatter), and $\sigma_{0,\text{veg}}$ is the backscattering coefficient from the vegetation volume.

Consider $\sigma_{0,\text{CR1}}$ of unobstructed CR1 and $\sigma_{0,\text{CR2}}$ of a similar reflector CR2 placed under the forest canopy (see Fig. 3). Assuming that $\sigma_{0,\text{CR1}} = \sigma_{0,\text{CR2}}$ and $\sigma_{0,\text{CR}} \gg \sigma_{0,\text{veg}}$, the observed σ_0 of CR2 through the forest canopy can be approximated as

$$\begin{aligned}\sigma_{0,\text{CR2,obs}} &= t_{\text{veg}}^2 \cdot \sigma_{0,\text{CR2}} + \sigma_{0,\text{veg}}\left(1 - t_{\text{veg}}^2\right) \\ &\approx t_{\text{veg}}^2 \cdot \sigma_{0,\text{CR1}}\end{aligned} \tag{2}$$

allowing to solve the canopy two-way attenuation L_{veg}^2

$$L_{\text{veg}}^2 = 1/t_{\text{veg}}^2 = \frac{\sigma_{0,\text{CR1}}}{\sigma_{0,\text{CR2,obs}}}. \tag{3}$$

It should be noted that (1) disregards effects such as multiple scattering within the canopy volume. Double-bounce effects from tree trunks (dashed line in Fig. 3) are not expected to significantly influence the point-like $\sigma_{0,\text{CR2,obs}}$.

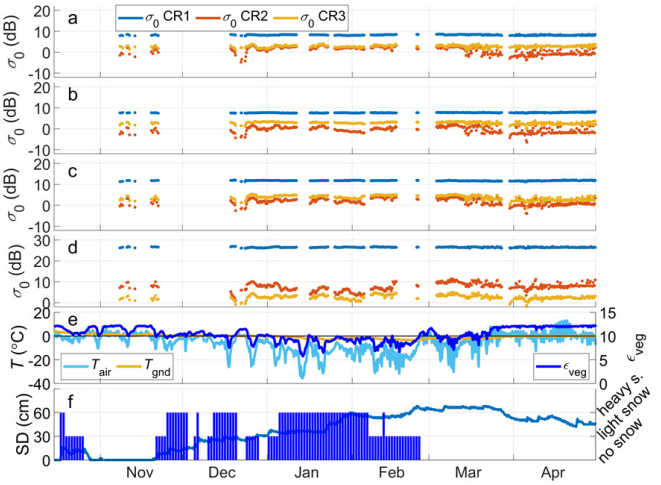

Fig. 4. Time series of σ_0 from CR1 (in open) and CR2 and CR3 (behind vegetation) at L-, S-, C-, and X-bands: (a)–(d) air temperature, ground temperature, and vegetation permittivity (e); SD on ground (SD) and presence of snow on canopy [no snow, light or heavy snow, (f)].

III. Results

A. Measured σ_0 of Corner Reflectors

Fig. 4(a)–(d) shows the time series of VV-pol σ_0 from the three CRs at the four observed bands. σ_0 from CR1 (after installation in the beginning of November 2020) can be seen to remain relatively stable throughout the experiment, with a peak-to-peak variability < 1.0 dB at L-band and < 1.3 dB at X-band. Larger variability can be observed for σ_0 measured from CRs 2 and 3, ranging from 7 dB at L-band to up to 9 dB at X-band.

Several maintenance breaks when the radar was not operating broke the time series, the longest intervals occurring between November 22 and December 18, 2020 as well as between February 16 and 24, 2021. Shorter breaks in the time series, e.g., in January 2021, represent periods when large changes were detected in CR1 backscatter, attributed to wet snow accumulation on the CRs. These data were removed from the analysis.

B. Environmental Conditions

Fig. 4(e) shows the observed air and ground temperatures (T_{air}, T_{gnd}) and vegetation permittivity ε_{veg}. SD, presence of canopy-intercepted snow (no snow, light snow, and heavy snow), is shown in Fig. 4(f).

T_{air} showed uninterrupted freezing temperatures from December 24, 2020 to February 25, 2021. The coldest measured T_{air} was $-35.7°$ on January 13, 2021, while T_{gnd} was below zero from December 28, 2020 to March 28, 2021. During winter, the maximum and minimum surface temperature of the trees T_{veg} (not shown in Fig. 4) followed T_{air} closely, albeit with a delay of 3–4 h; notable deviations start to occur only in April, most likely due to retained solar heating in the trees.

There was intermittent snow accumulation on the canopy from the first snowfall on October 17, 2020–February 25, 2021. The canopy was snow free from October 25 to November 21, 2021 when snow on the ground also melted. Melt

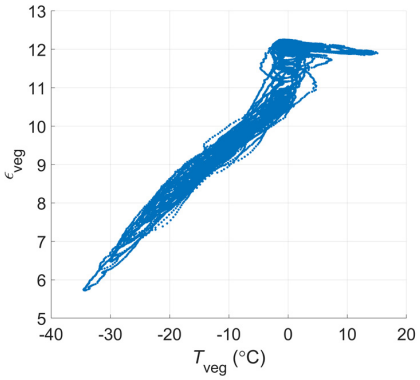

Fig. 5. Permittivity of wood ε_{veg} at 70 MHz against tree surface temperature T_{veg}, average of nine GS3 sensors.

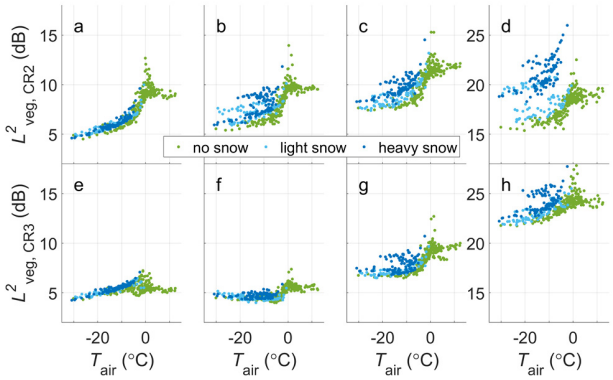

Fig. 6. Two-way attenuation L^2_{veg} of radar signal from (a)–(d) CR2 and (e)–(h) CR 3 at (a) and (e) L-, (b) and (f) S-, (c) and (g) C-, and (d) and (h) X-band against T_{air}. Light and heavy snow on canopy identified.

events on December 3, 7, 21 and 29, 2020 caused accumulated snow to fall from the branches. The canopy remained snow-free after February 25, 2021 despite minor snowfall events in March.

Fig. 5 shows ε_{veg} against T_{veg} as an average of the nine GS3 sensors. The relation shows a maximum measured permittivity at $T_{veg} \approx 0$ °C, with a rapid drop followed by monotonous decrease at $T_{veg} < 0$ °C. The temperature dependency at $T_{veg} > 0$ °C arises from the temperature dependency of free water, which is increasingly apparent around 0 °C [6]. The monotonous decrease of ε_{veg} for $T_{veg} < 0$ °C is hypothesized to be related to decrease of free water due to freezing of vegetation water in the trunks (see [5], [6]). The GS3 sensors measure permittivity at 70 MHz; the actual value of effective permittivity of water differs for higher frequencies. The mean standard deviation across the sensors was 0.85 for ε_{veg} and 0.3 °C for T_{veg}.

C. Estimated Two-Way Attenuation of Forest Canopy

Fig. 6 shows the two-way attenuation L^2_{veg} estimated from the measured backscatter of CR2 [Fig. 6(a)–(d)] and CR3 [Fig. 6(e)–(h)] using (3) against T_{air}. Cases where light or heavy snow was present on the canopy are identified (light and dark blue, respectively), compared to a snow-free canopy

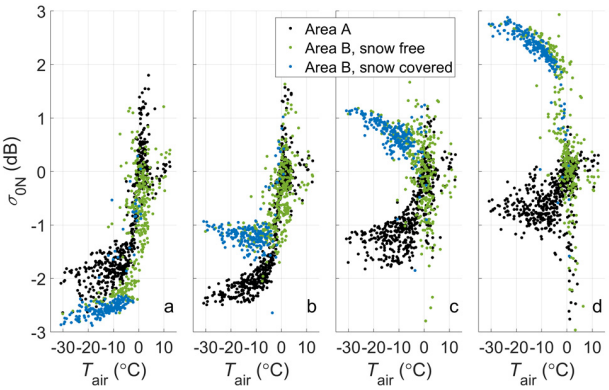

Fig. 7. σ_{0N} from Areas A and B (refer to Fig. 1) against T_{air} at (a)–(d) L-, S-, C-, and X-bands. σ_{0N} normalized to observed $< \sigma_0 >$ at $T_{air} > 5$ °C (summer conditions).

(green). Note that data in Fig. 6(d) and (h), representing X-band, have a different range.

For both CR2 and CR3, L^2_{veg} of a snow-free canopy (green) reached a maximum around $T_{air} \approx 0$ °C at all bands, with individual measurements showing even a 4-dB increase to mean summer levels. However, these measurements may be affected by refrozen snow or moisture on the CR surfaces. In winter, L^2_{veg} for CR2 decreased rapidly for $T_{air} < 0$ °C. Compared to the average attenuation in thawed conditions ($T_{air} > 5$ °C), the attenuation for CR2 decreased by ca. 4 dB at all bands when temperatures fell below −35 °C. For CR3, the decrease was more subdued, ranging from 1 dB at L-band to 2 dB at X-band, H. In thawed conditions, the overall attenuation from CR3 was weaker compared to CR2 from 4 dB at L-band to 8 dB at the C-band. The relation of L^2_{veg} to T_{veg} was highly similar to T_{air} (not shown).

For CR2(CR3), the effect of heavy snow cover increased the mean level of L^2_{veg} in frozen conditions ($T_{air} < -5$ °C) by 0.1(0.1), 1.2(0.2), 1.3(0.7), and 4.1(1.1) dB for L-, S-, C-, and X-bands, respectively. In particular, for CR2, the presence of snow increased L^2_{veg} above summer levels at the X-band. However, the variability from the effect of snow cover increased for higher frequencies, and the effect of light versus heavy snow was not clear in all cases.

For CR2, average L^2_{veg} increased from L- to X-band by 10 dB, while for CR3, the respective increase was 18 dB, due to high apparent attenuation at X-band. Contrary to lower frequencies, L^2_{veg} calculated from CR3 is greater than CR2 at the X-band; this is an indication of uncertainty in the CR orientation or in the compensation for antenna beam patterns, leading to uncertainty of the absolute magnitude of L^2_{veg}.

D. Backscatter From Bare Ground and the Forest Canopy

Fig. 7 shows the observed backscattering coefficient from Areas A and B against T_{air}, normalized to the mean of observations at $T_{air} > 5$ °C. The presence of snow on the canopy (either light or heavy snow) versus a snow-free canopy over Area B is distinguished using colors.

Backscatter from Area A decreased appreciably in winter at all bands. Comparing σ_0 at $T_{air} < -25$ °C to summer

conditions, the drop ranged from 2.1 dB at L-band to 0.7 dB at X-band. For Area B, σ_0 similarly decreased by ca. 2.7 dB at L-band and 1.0 dB at S-band. However, σ_0 from Area B at C and X-band in frozen conditions increased from 1.1 to 2.6 dB. Snow cover had no appreciable effect on σ_0 at any band, indicating snow mostly affected the total extinction in the canopy, instead of the backscattering from the vegetation itself [$\sigma_{0,\mathrm{veg}}$ in (1)].

IV. Discussion and Conclusion

In this study, the attenuation of the forest canopy was estimated by comparing the apparent σ_0 of trihedral CRs placed under the canopy to σ_0 of a CR with unobstructed line-of-sight to the radar. While the method is unable to directly separate changes in attenuation from changes in the backscatter of the canopy itself, this was estimated to be a minor source of error due to the relatively high σ_0 provided by the CRs; σ_0 observed from both obstructed CRs was above 10 dB compared to σ_0 of the forested Area B at all bands.

Two-way attenuation of a snow-free canopy at all bands was found to reach a peak around $T \approx 0$ °C (with respect to a peak in L-band VOD reported in [6]), followed by a monotonic decrease for $T < 0$ °C. With the exception of X-band, L^2_{veg} of a snow-free canopy from CR3 was 4–5 dB weaker compared to CR2, while winter-time dynamics of the signal were also weaker, due possibly to differing canopy properties in front of the CRs. However, at the X-band, the calculated L^2_{veg} was 4 dB greater for CR3, indicating possible uncertainties in either alignment of compensation for antenna gain at X-band, leading to increased uncertainty of L^2_{veg} at that frequency permittivity of the tree tissue, measured *in situ*, confirms the monotonic change of dielectric properties in freezing conditions, as well as a maximum permittivity measured around $T \approx 0$ °C (see Fig. 5). However, the measured change in permittivity is more linear in nature than the measured change in attenuation (see Fig. 6).

Although this study did not explicitly separate canopy backscatter from other components, the backscatter signatures measured from the forest canopy (see Fig. 7) resemble previous results obtained at the P-, C-, and X-bands ([12]–[14]) for canopy backscatter. The low impact of snow cover on backscatter intensity up to X-band also corroborates studies of snow on ground (e.g., [15]). The inverse response to temperature of canopy backscatter at the C- and X-bands, compared to L- and S-bands is hypothesized to be related to the response of different wavelengths to freezing of various components of the trees: at the C- and X-bands, decreased attenuation by smaller canopy components following freezing may have allowed an increased backscatter from larger canopy components (thicker branches, stem), whereas at the L- and S-bands, the attenuation of smaller canopy components was low regardless of canopy freezing, thus altering the backscatter less with freezing. The current setup did not allow to fully disentangle dielectric and structural effects on transmissivity and backscatter; a full physical explanation would require more study using a physical model identifying the impact of different components [16], including diffraction effects at different wavelengths, with supporting measurements characterizing the structure of vegetation. Generalization of the results would require further tests in forests of differing tree species, structure, and density.

The results of this study have implications for monitoring surface properties (e.g., snow and soil) using SAR. Furthermore, the results affect estimates of the capability of SAR instruments to detect objects with a high RCS beneath the canopy in winter.

References

[1] T. Le Toan *et al.*, "The BIOMASS mission: Mapping global forest biomass to better understand the terrestrial carbon cycle," *Remote Sens. Environ.*, vol. 115, no. 11, pp. 2850–2860, 2011, doi: 10.1016/j.rse.2011.03.020.

[2] A. Beaudoin *et al.*, "Retrieval of forest biomass from SAR data," *Int. J. Remote Sens.*, vol. 15, no. 14, pp. 2777–2796, Sep. 1994, doi: 10.1080/01431169408954284.

[3] S. Saatchi, "SAR methods for mapping and monitoring forest biomass," in *SAR Handbook: Comprehensive Methodologies for Forest Monitoring and Biomass Estimation*. A. Flores, K. Herndon, R. Thapa, and E. Cherrington, Eds. NASA, 2019, doi: 10.25966/hbm1-ej07.

[4] P. Ferrazzoli, S. Paloscia, P. Pampaloni, G. Schiavon, S. Sigismondi, and D. Solimini, "The potential of multifrequency polarimetric SAR in assessing agricultural and arboreous biomass," *IEEE Trans. Geosci. Remote Sens.*, vol. 35, no. 1, pp. 5–17, Jan. 1997, doi: 10.1109/36.551929.

[5] Q. Li *et al.*, "The influence of thermal properties and canopy-intercepted snow on passive microwave transmissivity of a scots pine," *IEEE Trans. Geosci. Remote Sens.*, vol. 57, no. 8, pp. 5424–5433, Aug. 2019, doi: 10.1109/TGRS.2019.2899345.

[6] M. Schwank *et al.*, "Temperature effects on L-band vegetation optical depth of a boreal forest," *Remote Sens. Environ.*, vol. 263, Sep. 2021, Art. no. 112542, doi: 10.1016/j.rse.2021.112542.

[7] W. Havranek and W. Tranquillini, "Physiological processes during winter dormancy and their ecological significance," in *Ecophysiology of Coniferous Forests*, W. Smith and T. Hinckley, Eds. San Diego, CA, USA: Academic, 1995, pp. 95–117.

[8] A. Lintunen, T. Hölttä, and M. Kulmala, "Anatomical regulation of ice nucleation and cavitation helps trees to survive freezing and drought stress," *Sci. Rep.*, vol. 3, no. 1, pp. 1–7, Dec. 2013, doi: 10.1038/srep02031.

[9] J. J. Ruiz *et al.*, "SodSAR: A tower-based 1–10 GHz SAR system for snow, soil and vegetation studies," *Sensors*, vol. 20, no. 22, p. 6702, Nov. 2020, doi: 10.3390/s20226702.

[10] R. Tarvainen, "Männyn lehtialaindeksin ja biomassan mallinnus SodSAR-tutkalla (in Finnish)," M.S. thesis, Fac. Sci. Forestry, School Forest Sci., Univ. Eastern Finland, Joensuu, Finland, 2021. [Online]. Available: http://urn.fi/urn:nbn:fi:uef-20210927

[11] E. P. W. Attema and F. T. Ulaby, "Vegetation modeled as a water cloud," *Radio Sci.*, vol. 13, no. 2, pp. 357–364, Mar. 1978, doi: 10.1029/RS013i002p00357.

[12] A. R. Monteith and L. M. H. Ulander, "Temporal characteristics of P-band tomographic radar backscatter of a boreal forest," *IEEE J. Sel. Topics Appl. Earth Observ. Remote Sens.*, vol. 14, pp. 1967–1984, 2021, doi: 10.1109/JSTARS.2021.3050611.

[13] J. Cohen *et al.*, "The effect of boreal forest canopy in satellite snow mapping—A multisensor analysis," *IEEE Trans. Geosci. Remote Sens.*, vol. 52, no. 6, pp. 3275–3288, Jul. 2015, doi: 10.1109/TGRS.2015.2444422.

[14] J. Cohen *et al.*, "A modeling-based approach for soil frost detection in the northern boreal forest region with C-band SAR," *IEEE Trans. Geosci. Remote Sens.*, vol. 57, no. 2, pp. 1069–1083, Feb. 2019, doi: 10.1109/TGRS.2018.2864635.

[15] S. Leinss, A. Wiesmann, J. Lemmetyinen, and I. Hajnsek, "Snow water equivalent of dry snow measured by differential interferometry," *IEEE J. Sel. Topics Appl. Earth Observ. Remote Sens.*, vol. 8, no. 8, pp. 3773–3790, Aug. 2015, doi: 10.1109/JSTARS.2015.2432031.

[16] F. T. Ulaby, K. Sarabandi, K. McDonald, M. Whitt, and M. C. Dobson, "Michigan microwave canopy scattering model," *Int. J. Remote Sens.*, vol. 11, no. 7, pp. 1223–1253, 1990, doi: 10.1080/01431169008955090.